NUCL SCI TECH (2020) 31:38
https://doi.org/10.1007/s41365-020-0747-3

Conceptual design of irradiation device for silicon neutron transmutation doping around Es-Salam research reactor

M. Salhi[1] · B. Mohammedi[1] · S. Laouar[1] · M. Dougdag[1] · M. Touiza[1] · M. Abbaci[2] · M. Moughari[1]

Received: 12 November 2019 / Revised: 11 February 2020 / Accepted: 12 February 2020 / Published online: 18 March 2020

Abstract Silicon neutron transmutation doping remains one of the most viable nuclear applications for research reactors. Providing this kind of product involves an irradiation method capable of fulfilling the quality requirements of doping and alleviating the challenges related to the design and safety of the irradiation device. In this paper, we propose an irradiation device prototype for neutron transmutation doping of silicon ingots with diameters of 2 to 3 in. based on the Es-Salam research reactor. The thermal hydraulic analysis of the proposed irradiation device was performed to determine the optimum conditions for cooling. The effect of the mechanical vibrations induced by the circulation of coolant in the device was quantified via experimental measurements under different flow rates. The results show that the maximum temperature reached by the silicon ingots is below the temperature limit, effectively validating the design of the irradiation device. Other investigations are prospected to further optimize the design and the irradiation conditions. The irradiation of silicon ingots with a large diameter will be considered.

Keywords Irradiation device prototype · Es-Salam research reactor · NTD-Si · Irradiation temperature · CFD method

1 Introduction

Neutron transmutation doping of *n*-type silicon single crystals (NTD-Si) allows the fabrication of a phosphorus-doped semiconductor material with low electrical resistivity and a volume homogeneous distribution of less than 5%, which is lower than that obtained using conventional doping chemical methods [1]. The NTD-Si process is based on the conversion of Si-30 isotope into a phosphorus atom via neutron absorption. The concentration of the P-31 doped in this process is a function of the Si-30 concentration, neutron capture cross section of the transmutation reaction, and neutron fluence. The capture microscopic cross section of this reaction is about 1.1×10^{-29} m^2 for highly thermalized neutrons. The final resistivity depends on pre-doping resistivity (initial resistivity), neutron fluence, and the doping coefficient which depends on the reactor type.

The quality obtained from this process enables the manufacturing of large and high power electronics components used in different domains (automotive industry, rail vehicles, and power engineering electronics including power distribution and power devices, such as thyristors, rectifiers, IGBT's, and power MOSFET's). In these last few years, following the increasing demand especially due to the development of hybrid cars, manufacturing was oriented toward the irradiation of large diameter ingots (6 to 8 in) instead of medium diameter ingots (3 to 5 in.). Nevertheless, some research reactors (RRs) still produce

This work was supported by the Nuclear Research Centre of Birine of Algerian Atomic Energy Commission.

✉ M. Salhi
mn_salhi@yahoo.fr

1 Centre de Recherche Nucléaire de Birine, 17200 Ain Oussera, Algeria

2 Institut Algérien de formation en Génie Nucléaire, 16050 Draria, Alger, Algérie

low diameter doped silicon for their local markets. This trend encouraged nuclear designers to update existing NTD-Si irradiation devices (BR2, SAFARI-1, FRM II) [2, 3] or to fabricate new RRs dedicated to this kind of nuclear application (JHR, OPAL, CAAR) [3].

The design of NTD-Si irradiation devices differs from one reactor to another [4–10]. For instance, it is more convenient and flexible for pool-type reactors than for tank-type reactors, owing to constraints related to irradiation, cooling, loading/unloading and transfer, change in ingot positions among others. In order to avoid permanent radiation damage in the crystal lattice by fast neutron ($E \geq 1$ MeV) and energy deposition by gammas even after annealing [11, 12], the thermal-neutron flux in the irradiation position should be several times higher than the fast neutron flux (at least a ratios order of few tens, hence a heavy water research reactor is more suitable). A thermal-to-fast neutron flux ratio of 7:1 was recommended in the IAEA consultants meeting (IAEA-TECDOC-1681, 2012), and the irradiation temperature should be maintained at a low level to prevent the silicon from reaching the temperature limit of 453.15 K. The spatial variation in the neutron flux density should be approved in order to obtain a symmetrical flatten flux within a large possible length; several methods were used to achieve this requirement, namely vertical motion, rotation of ingots, variable thickness absorber screens (stainless steel, titanium, nickel, etc.), graphite reflector blocks to eliminate flux distortion, minimizing ingots length, and intermittently changing the irradiation positions of silicon ingots. The maximum radial neutron flux variation is defined as the ratio of the difference between the maximal neutron flux and minimum neutron flux to the minimum neutron flux. A value of less than 10% is best for radial homogenous doping [8].

Considering the possible surface contamination of silicon ingots during irradiation, tight containers and simple baskets are used to hold silicon ingots.

The design of irradiation must also meet the safety requirements of the reactor. The loading of fresh ingots to and the unloading of irradiated ingots from the irradiation rig is carried out without shutting down the reactor, so reactor safety should be taken into account. For example, the reactivity influence on reactor operation should be determined.

N-type single-crystal silicon samples with initial resistivity of 100 Ω cm were irradiated under various neutron fluences in the vertical experimental channel situated in the heavy water reflector region of the Es-Salam research reactor. Radiation defects were investigated and removed by annealing [13]. Osmani et al. [14] fabricated a boron-doped Czochralski-silicon single crystal ($\rho = 2\ \Omega$ cm) on *P*-type small samples with crystal growth orientation at (100). These samples were irradiated at the neutron fluences 1.98×10^{18} and 3.96×10^{18} n/cm^2 in the D_2O moderator region of the Es-Salam reactor, and isochronal annealing under argon atmosphere was carried out up to 950 °C. Divacancy concentration and center radiation defects disappeared after annealing, and the doping was homogenous. They demonstrated that the transmutation of boron to lithium can be accomplished in the Es-Salem reactor irradiation.

These experimental results complemented the basis for the design of an irradiation device for producing silicon ingots.

In this work, authors present a conceptual design of an irradiation rig for the neutron transmutation doping of two silicon ingots with a diameter of 2 in (50.8 mm) and a total length of 400 mm. A prototype was created to verify the design by conducting some mechanical performance tests.

Coolant-induced vibrations were evaluated experimentally in order to acquire the optimal flow rate.

Thermal hydraulic analysis of the two silicon ingots, irradiated in two different regions of the Es-Salam reactor core, was conducted. For this purpose, a computational fluid dynamics (CFD) numerical model was developed to predict the maximum temperature under various conditions of compressed air coolant. Finally, the streamlines of the compressed air coolant at different flow rate were investigated.

2 NTD-Si irradiation device

2.1 Design and structure of the irradiation device

Es-Salam is a multipurpose heavy water research reactor (MHWRR), cooled and moderated using heavy water and a graphite as the reflector. It is a tank type with a nominal power of 15 MW. Its maximum thermal-neutron flux reaches 2.4×10^{14} n/cm^2 s at the central irradiation channel position. The availability of a flat neutron flux and low nuclear heating in the heavy water and graphite reflector satisfy the requirements of several types of irradiation. The rather large core of the Es-Salam enables a high slowdown of fast neutrons. Moreover, the thermal-to-fast neutron flux ratio is higher farther from the core.

The design of the reactor has been optimized to satisfy radioisotopes and doped silicon productions requirements, to supply high-flux neutron beams for researchers. The reactor has quite a pure thermal–neutron spectrum and a large space available for arranging many vertical and horizontal channels. There are more than 40 dry vertical irradiation channels with 3 different diameters disposed in different regions, 2 pneumatic irradiation devices that are dedicated to neutron activation analysis and delay neutron counting, 5 horizontal beam radial channels, and a thermal column [15].

The irradiation device prototype, as illustrated in Fig. 1a, is designed to ensure the irradiation of cylindrical silicon ingots with diameters of 2 to 3 in.; it was adapted to the vertical experimental channels situated either in the heavy water reflector region or in the graphite reflector region of the Es-Salam research reactor core. The device consisted of two concentric aluminum thin tubes: The inner one is coupled to a rotating driven system, and the outer one is motionless and used to ensure the circulation of the coolant and as a thermal barrier against the reactor core. Two silicon ingots with a length of 200 mm are introduced in the aluminum containers and placed remotely on the bottom of the rotating tube using a top cabinet cantilever.

Graphite blocks can be used to place silicon ingots in a suitable vertical position and avoid any possible neutron flux depression. An annular space of 3/4 of circle, located opposite to the reactor core, is envisaged between the rotating tube and the fixed tube to locate the gammas attenuation materials or neutron absorber materials for axial neutron flux flatting. A neutron flux measuring system is connected to the device for on line integrated thermal-neutron flux measurement. The device is accommodated to ensure remote loading/unloading and, eventually, position change of the silicon containers using the cantilever of the reactor top cabinet.

The rotating driven system of the irradiation device is composed of a 0.75-KW asynchronous motor which has a maximum rotating velocity of 996 rpm, a gear mechanism, variable speed drives ATP-16U18N4, and a tachometer. This system provides a precise rotating speed in the range of 0 to 10 rpm.

The neutron measuring system is comprised of two rhodium-103 self-powered neutron detectors (SPND) with a sensitivity 5.6×10^{-21} A/cm^2 s and a 4695 A Studsvik amplification module, which has a nominal amplification factor of 0.5×10^7 V/A by channel.

A control command system, based on the client server architecture with TCP/IP communication liaison, provided through a Labview exploitation program was developed to remotely command and supervise the principal parameters of the silicon doping operation.

2.2 Mechanical performances tests of the prototype

In order to address the challenge of safety for the Es-Salam reactor, as in real use, a prototype of the irradiation device at a reduced scale was fabricated with all necessary auxiliary systems. The main goal of this process is to

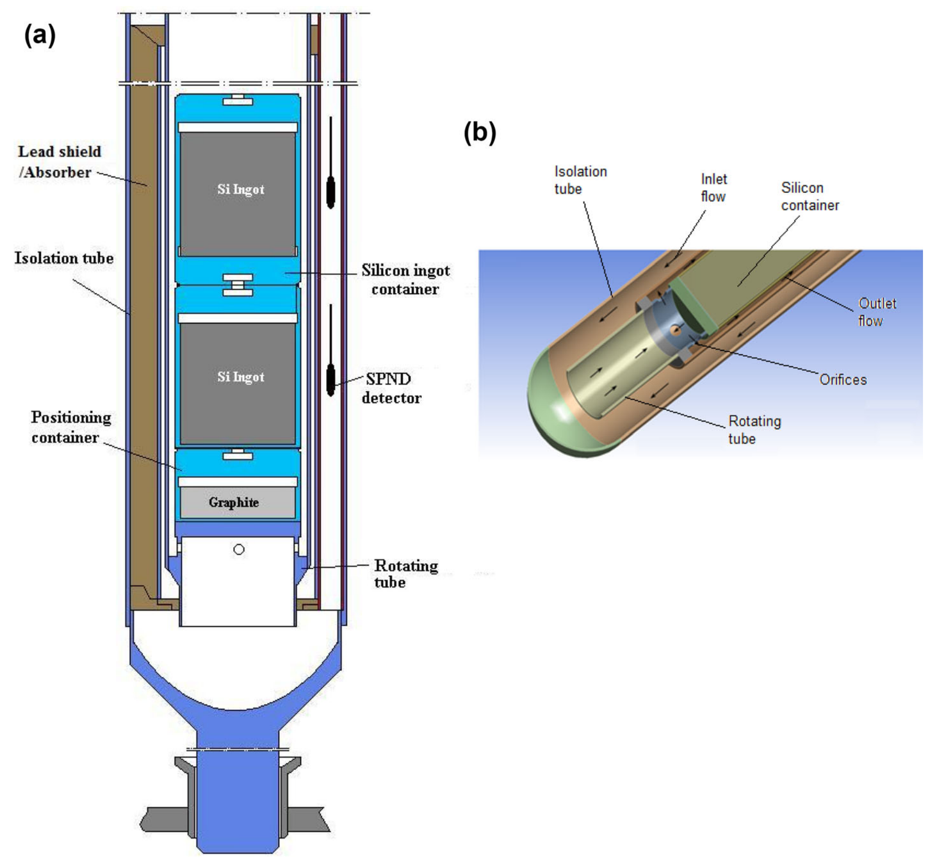

Fig. 1 NTD-Si irradiation device: **a** mechanical structure of an NTD-Si device, **b** flow path of coolant at the bottom of an NTD-Si irradiation device (color online)

enable the performance of a series of out of pile qualification tests in normal operation conditions. One of the tests verifies the operation and identifies its mechanical performances.

Unfortunately, the presence of singularities; the cross-section change of the coolant passage, which involves a variation of coolant flow velocity; and the direction changes of coolant inside the irradiation rig generate pressure drops and could disturb the normal circulation of the coolant. Considering the interaction of fluid structure and the mechanical forces caused by the rotation driven system, all those phenomena and events could threaten the integrity of the NTD-Si irradiation device and its vicinity.

To quantify the impact of those factors on the conceptual design of the NTD-Si irradiation device, experimentation tests were conducted on the prototype during its operation.

This qualification was done in order to ensure that the design is reliable from points of view of operability, mechanical, and hydraulic behaviors. It is also a way of checking whether the irradiation device operation parameters generate strains and stresses above the limitation values. Furthermore, it is a helpful step in enhancing the design and bringing technical solutions in case of malfunctions.

As illustrated in Fig. 2a, the prototype was fixed on a rigid carbon steel platform in the similar assembly conditions as that on the reactor core. It is connected to an instrumented compressed air coolant circuit composed mainly of a three-piston compressor, which delivers a maximum flow rate of 60 m^3/h and a maximum pressure of 7 bar, a tank with a volume of 1 m^3 equipped with safety valve and battery of filters (vapors oil and dust filters), a flow meter, two pressure gauges for the measurement of the inlet and outlet pressures of coolant inside the irradiation device, an anemometer, a pressure reducing valve to regulate the pressure at the entry of the irradiation device, and a set of check and throttle valves.

A vibration system was used to measure the vibrations at various positions of the prototype under operation conditions of pressure, which varied from 3 to 7 bar, and the coolant velocity of compressed air at the exit part of the irradiation device was varied from 2.5 to 35 m/s. Based from practical knowledge, about 13 points of measurement were chosen. The points were chosen based on the connecting points between parts, fixation points, and maximum displacement, which can occur on the tube. Among those points, seven were along the tube in order to describe the deformation.

This vibration measurement system is comprised of sensors (accelerometers and force transducer), amplifiers and hammer (Brüel and Kjær) [16, 17], a laptop with a PCMCIA card, and a home software (DAQ700) for signal treatment and vibration analysis. For the test method, the choice was done on the impact hammer instead of the electrodynamics exciter. In order to reduce errors, measurements were done several times from 5 to 10 times, taking the average values [16–18].

The vibrational inspection of the prototype behavior under different operation conditions (pressure, flow rate of compressed air coolant, and velocity of rotating tube of the irradiation rig) reveals that the operation is normal, the noise level is weak and lower than 50 dB, small mechanical frictions are present, the motion transmission system is

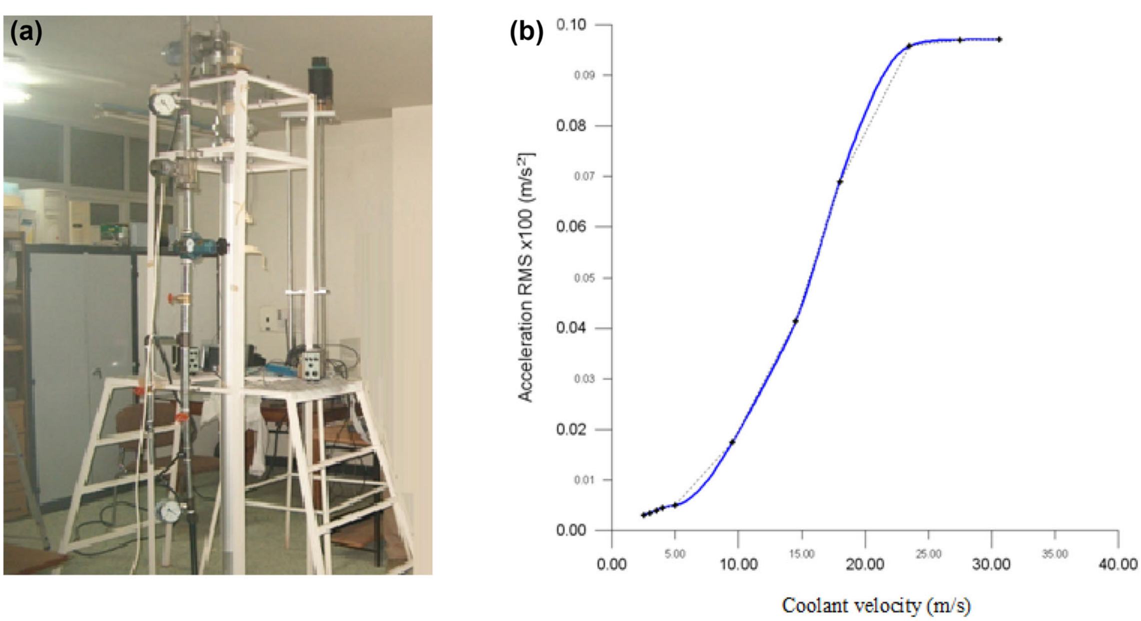

Fig. 2 **a** Experimental setup of the NTD-Si prototype, **b** acceleration versus coolant velocity (color online)

adequate and reliable, and the circulation of compressed air inside the irradiation device is appropriate.

Vibration measurements, as illustrated in Fig. 2b, show that there is a direct correlation between acceleration and compressed air flow rate; however, a slight range of stability is observed at high coolant velocity up to 23 m/s, where an acceleration about 1 m/s^2 is obtained. This maximum acceleration is quite weak, and the equivalent generated forces do not produce harmful mechanical stresses, remaining less than the allowable stress for the irradiation device material (aluminum 6061, $\sigma_{adm} = 87$ MPa [19]).

In parallel, a numerical model was elaborated and validated using the obtained experimental data. The model is extended to simulate the irradiation device at a real scale. The results of the simulation at static and dynamic mode show a stress of about 2 MPa [19] which is less than the limits as shown previously. These results prove the robustness of the model in spite of the severe conditions applied.

3 Thermal hydraulic analysis

3.1 Heat source and cooling process

Nuclear heat generation in a non-fissile bulk and high-density material in or near the reactor core comes mainly from the energy deposited by the collision and interaction of primary gammas (fission gammas and fission product decay gammas that constitute 2/3 of the total gammas released in the core) and from, at a less degree, secondary gammas (resonance, thermal absorption, and inelastic scattering) [20–22]. According to the type and the power of the reactor and irradiation position in the core, gamma heat on silicon varies in the range of 0.02 to 0.5 W/g. Previous studies [1, 23] found that heat densities of 0.02 W/g and 0.25 W/g are generated, respectively, in 3-in.-diameter silicon irradiated in the graphite reflector region and in 4-in.-diameter silicon irradiated in heavy water reflector region of a DR3 research reactor, considering that DR3 is 10-MW tank-type reactor cooled and moderated with heavy water.

Koziel and Pytel [24] found that a heat density of 0.25 W/g is generated in 2-in.-diameter silicon irradiated in the light water reflector region of the EWA research reactor (EWA is a 10-MW tank-type reactor cooled and moderated with light water). They also mentioned that a heat density of 0.5 W/g is generated in 3-in.-diameter silicon irradiated in the graphite reflector region of the MARIA research reactor (MARIA is a 30-MW power pool reactor cooled with light water and moderated with light water and beryllium).

Kim et al. [25] experimentally measured the nuclear heat on aluminum samples around the experimental channels of the HANARO research reactor through the calorimetric method. They obtained a nuclear heat density of 0.143 W/g at the power of 8 MW and prospected a nuclear heat density of 0.473 W/g at the full power of 30 MW (HANARO is a 30-MW pool-type reactor cooled and moderated with light water).

Under gamma and neutron radiations, all structural materials of the NTD facility become sources of heat. In the present paper, only the heat generated from the two silicon ingots was considered in the thermal hydraulic analysis. We assume, for both irradiation positions, a heat density of 0.25 W/g as heat source generated in the 2-in. silicon ingot irradiated inside the NTD-Si irradiation device prototype. The maximum temperatures in the vertical experimental channel situated in graphite reflector region and in the vertical experimental channel located in heavy water reflector region of the Es-Salam core were 393.15 and 343.15 K, respectively.

Compressed air, in an open cycle mode, is considered as a coolant that removes nuclear heat from the structural material of the irradiation device and silicon ingots. This coolant is selected for its low void coefficient, because the heat source is weak, and to facilitate loading and unloading operations.

The argon-41 concentration (half-life of 109.2 min) generated by the activation and irradiation of air through the nuclear reaction $^{40}Ar\ (n,\gamma)\ ^{41}Ar$ mainly contributes to the total activity of air. Trace Ar-40 of 0.933% by air volume activates with a thermal capture cross of 0.7 barn and emits a gamma ray of 1294 keV. This phenomenon was considered in the design to keep the dose rate below the limits. The use of light or heavy water as coolant requires a complicated design, an important investment cost (irradiation device, thermal–hydraulic loops, loading/unloading, and transfer system), and can cause neutron flux distortion. Filtered compressed air with a temperature of 393.15 K and a pressure of 3 bar was introduced at the top part of the irradiation device. It circulates between the inner wall of the isolation tube and the outer wall of the rotating tube until the hemispherical part where it emerges through the four circular holes, toward the annular section constituted between the inner wall of the rotating tube and the outer walls of the silicon containers. Thus, it carries out heat transfer by the forced convection phenomena between the air coolant and silicon ingots (Fig. 1b).

Three-dimensional temperature distributions of the two irradiated silicon ingots, as well as the flow path of coolant through the singular points of the irradiation rig (holes, hemispherical part, direction change, etc.), were calculated for three flow rates, 10, 20, and 30 m^3/h, and in both

Table 1 Irradiation conditions and thermal hydraulic parameters

Parameters and conditions	Heavy water reflector	Graphite reflector
Irradiation site		
Mean neutron thermal flux (n/cm^2 s)	10^{13}	10^{12}
Ratio $\Phi_{th}(E > 1\ \text{MeV})/\Phi_f$	30	300
Gamma heating (W/g)	0.25	0.25[a]
Structural material of irradiation device	Al alloy 6061	Al alloy 6061
Coolant	Air	Air
Coolant pressure (bar)	3	3
Coolant inlet temperature (°C)	20	20
Coolant flow rate (m^3/h)	10, 20, 30	10, 20, 30
Site environment temperature (°C)	70	120
Si ingot		
Number	2	2
Diameter (mm)	50.8	50.8
Length (mm)	200	200
Medium	Helium gas	Helium gas

[a] 0.25 W/g is a conservative value because the gamma heat generated in the materials at this location, far from reactor core, is absolutely lower than that in regions near the core

irradiation sites. Table 1 summarizes the irradiation conditions and the thermal hydraulic parameters considered.

3.2 Governing equations

To study the characteristics of cooling effect on the target by varying the inlet air mass flow, the governing equations of continuity, momentum, and energy are expressed as follows [26, 27]:

$$\frac{\partial \rho}{\partial t} + \nabla(\rho \vec{v}) = S_m, \tag{1}$$

where S_m is the mass added to the continuous phase from the dispersed second phase and any user-defined sources.

$$\nabla(\rho \vec{v}\vec{v}) = -\nabla p + \nabla\left(\bar{\bar{\tau}}\right) + \rho \vec{g} + \vec{F}, \tag{2}$$

where p is the static pressure, $\bar{\bar{\tau}}$ is the stress tensor, and $\rho\vec{g}$ and $\vec{F}$ are the gravitational body force and external body forces, respectively.

$$\nabla(\vec{v}(\rho E + p)) = \nabla\left(k_{\text{eff}} \nabla T + \left(\bar{\bar{\tau}}_{\text{eff}} \vec{v}\right)\right) + S_h, \tag{3}$$

where k_{eff} is the effective conductivity. The first two terms on the right-hand side of Eq. (3) represent energy transfer due to conduction and viscous dissipation, respectively. S_h is the volumetric heat source.

3.3 Turbulence model

Two-equation turbulence models allow the determination of both turbulent length and timescale by solving two separate transport equations. The standard $k-\varepsilon$ model in ANSYS Fluent falls within this class of models and has become the workhorse of practical engineering flow calculations since it was proposed by Launder and Spalding.

The turbulence kinetic energy, k, and its rate of dissipation, ε, are obtained from the following transport equations [26, 27]:

$$\frac{\partial}{\partial t}(\rho k) + \frac{\partial}{\partial x_i}(\rho k u_i) = \frac{\partial}{\partial x_j}\left[\left(\mu + \frac{\mu_t}{\sigma_k}\right)\frac{\partial k}{\partial x_j}\right] + G_k + G_b - \rho\varepsilon - Y_M + S_k, \tag{4}$$

and

$$\frac{\partial}{\partial t}(\rho \varepsilon) + \frac{\partial}{\partial x_i}(\rho \varepsilon u_i) = \frac{\partial}{\partial x_j}\left[\left(\mu + \frac{\mu_t}{\sigma_\varepsilon}\right)\frac{\partial \varepsilon}{\partial x_j}\right] + C_{1\varepsilon}\frac{\varepsilon}{k}(G_k + C_{3\varepsilon}G_b) - C_{2\varepsilon}\rho\frac{\varepsilon^2}{k} + S_\varepsilon, \tag{5}$$

where G_k represents the generation of turbulence kinetic energy due to the mean velocity gradients, calculated as described in the modeling turbulent production in the $k-\varepsilon$ models. G_b is the generation of turbulence kinetic energy due to buoyancy, calculated as described in effects of buoyancy on turbulence in the $k-\varepsilon$ models. Y_M represents the contribution of the fluctuating dilatation in compressible turbulence to the overall dissipation rate, calculated as described in effects of compressibility on turbulence in the $k-\varepsilon$ models. $C_{1\varepsilon}$, $C_{2\varepsilon}$, $C_{3\varepsilon}$, and C_μ are constants. σ_k and σ_ε are the turbulent Prandtl numbers for k and ε, respectively. S_k and S_ε are user-defined source terms.

The turbulent (or eddy) viscosity μ_t is computed by combining k and ε as follows:

$$\mu_t = \rho C_\mu \frac{k^2}{\varepsilon}. \quad (6)$$

3.4 Numerical modeling

Computational fluid dynamic method (CFD), by means of ANSYS Fluent version 14.5, is utilized to simulate the thermal hydraulic behavior of silicon ingots inside the irradiation device prototype. This is justified by the fact that this method is useful and efficient for describing the local behavior of fluid flow and heat transfer. It also gives a detailed visualization of flow and temperature distribution at any point of the studied domain. The CFD codes solve the transports equations (conservation of mass, momentum, and energy [26]), which are discrete with the finite volume method (FVM), governing these physical phenomena. The $k-\varepsilon$ standard turbulence flow model is considered for the analysis of heat transfer and the flow streams of compressed air in different regions of the simulation domain. The problem is treated as a steady-state mono-phase turbulent flow. The structured meshing type adopted is dominant for the geometry model. In order to compare the dependency of the calculated physical parameters (as example temperatures) on grid size, several densities of grid were tested to obtain the appropriate one which ensures minimum uncertainties (1,208,906 nodes and 1,973,701 elements). A difference of 1% between two consecutive results of calculated physical parameters (as example temperatures) is considered as the selection criterion of the adopted grid [27].

4 Results and discussions

The simulation of thermal hydraulic behaviors, under different cases, has led to the following results.

Figure 3 shows the evolution of the hottest silicon ingot temperature versus time for a coolant at zero flow rate. It should be noted that the temperature increases promptly to reach the value of 950 K after an irradiation time of 2 h, which is much higher than the limit temperature. The obtained result justifies the necessity for the use of the proposed cooling system and confirmed that natural convection is not enough to dissipate the heat generated in the silicon ingots.

Figure 4 shows the contour of the temperature of different components in the irradiation device prototype at the heavy water reflector position cooled with compressed air at the flow rate of 30 m^3/h. It was observed that most parts of the upper silicon ingot reached a maximum temperature

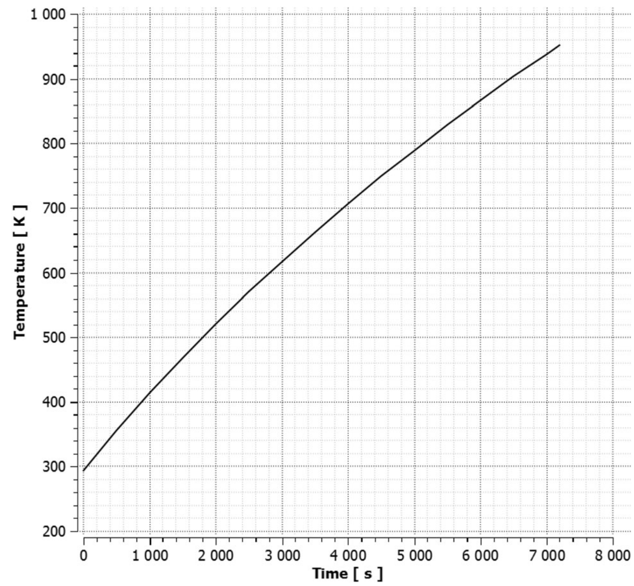

Fig. 3 Hottest silicon ingot temperature evolution versus time

of 374.12 K which is below the limit value. At the low coolant flow rate of 10 m^3/h and in the same irradiation position, the maximum temperature of the hot silicon ingot was of 439.97 K.

Figure 5 presents the radial profile temperature at the top level of the hot silicon ingot for the three compressed air flow rates, 10, 20, and 30 m^3/h. It was observed that the temperatures of this silicon ingot were homogeneous along the diameter and drastically decrease at the helium gap inside the silicon ingot container to reach a mean temperature of 315 K at the annular section between the external wall of the container and the internal wall of the rotating tube. The obtained results validate our design and show clearly the positive effect of the helium gas gaps which led to a homogeneous heat dissipation inside silicon ingots, a small variation of temperatures between the centerline and the peripheral sides of the two silicon ingots, the absence of hot points, and an efficient thermal isolation between the irradiation device and the irradiation channel. A temperature difference of 15 °C was obtained between the inlet and outlet coolant temperatures across the two irradiated silicon ingots.

Figure 6a shows the velocity streamlines of the cooling compressed air at singular points of the irradiation device prototype. The cooling fluid was roughly slow approaching the contact surfaces of the hemispherical part of fixed tube, and the area in the central region was undersupplied. Thereafter, a normal increase in the coolant velocity was recorded due to the change of cross-sectional area at the entrance of the rotating tube. The maximum coolant velocity of 34.96 m/s was reached for the coolant flow rate of 30 m^3/h at the entrance of the fourth rotating tube hole

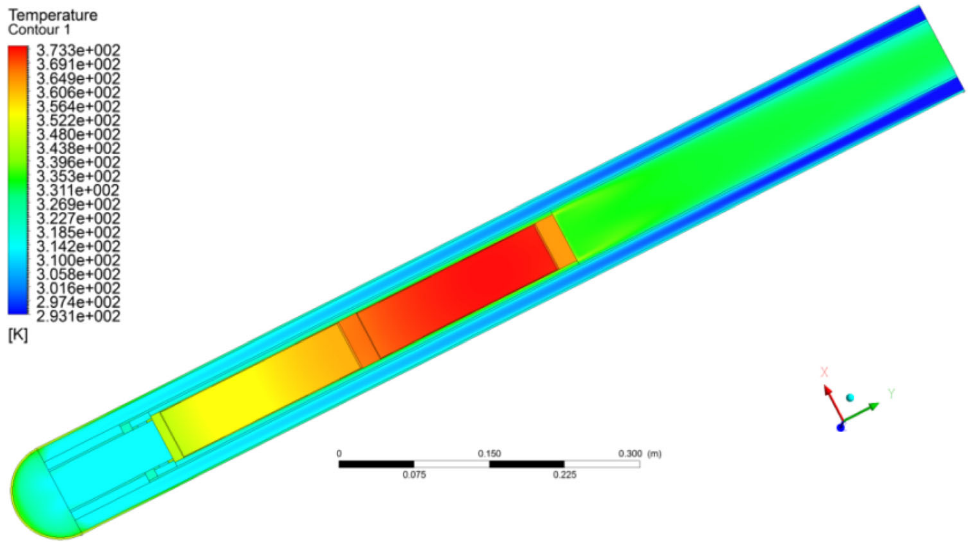

Fig. 4 Contour of temperature distribution at a coolant flow rate of 30 m^3/h (heavy water reflector region) (color online)

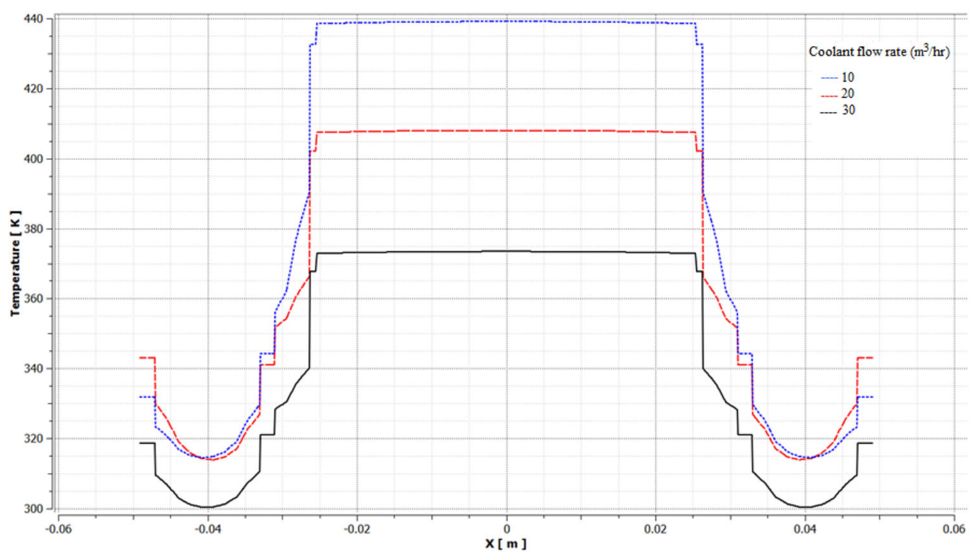

Fig. 5 Radial temperature profile at the top level of the hot silicon ingot for 10, 20, and 30 m^3/h (heavy water reflector irradiation position) (color online)

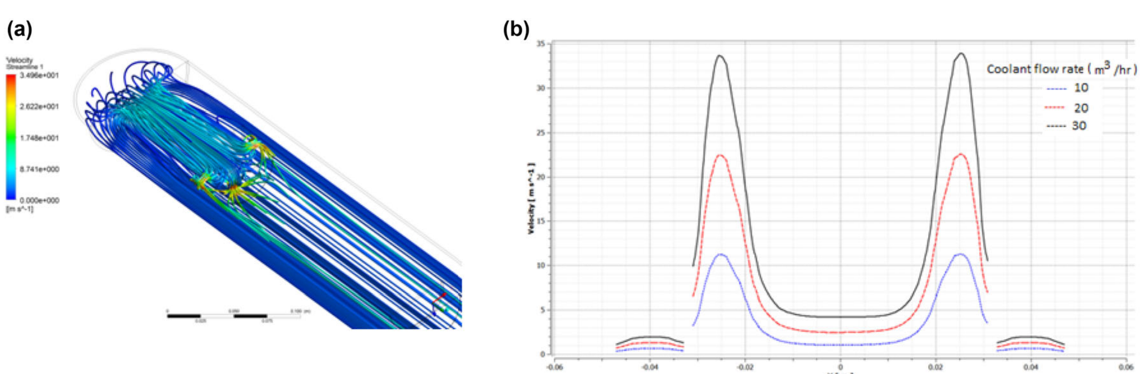

Fig. 6 **a** Velocity streamlines at singular points of the irradiation device at the flow rate of 30 m^3/h, (color online), **b** radial profile of velocity at holes for flow rates of 10, 20, and 30 m^3/h

Table 2 Maximum temperatures and coolant velocities at different coolant flow rates

Irradiation position	Coolant flow rate (m^3/h)	Silicon maximum temperature (K)	Maximum coolant velocity (m/s)
Heavy water reflector	10	439.97	12.17
	20	408.76	24.71
	30	374.12	34.96
Graphite reflector	10	452.37	12.17
	20	438.54	24.71
	30	393.15	34.96

(Fig. 6b). In the annular space between the external walls of the silicon ingot containers and the inner walls of rotating tube, the velocity of the coolant was about 17.48 m/s.

Table 2 summarizes, for both irradiation positions in the reactor core, the maximum silicon ingot temperatures and coolant velocities in the entrance of the rotating tube orifices for the coolant flow rates of 10, 20, and 30 m^3/h. It appears that, considering all coolant flow rates, the second silicon ingot reaches a maximum temperature below the limit. The coolant velocities obtained do not disturb the normal flow inside the singular points in the irradiation device.

The appropriate coolant flow rate of the silicon ingots depends also on other external factors that avoid the limit temperature, mainly the radioactive nuclide argon-41. The amount of argon-41 is inversely proportional to the flow rate of the coolant inside the irradiation device. A depth evaluation of the activity showed a possible contamination. Therefore, it is important to determine the maximum amount which could be expelled to the atmosphere and the capacity of the ventilation system (air changes rate) of the reactor to remove radioactive nuclide argon-41 from the irradiation device in order to validate the design, enhance it, or consider other alternative solutions. As discussed above, the allowable coolant flow rates do not induce harmful vibrations of the irradiation components.

5 Conclusion

A conceptual design of an irradiation device for neutron transmutation doping of silicon based on the Es-Salam research reactor is done. The design of this device was qualified by conducting some performance tests on a prototype. The results demonstrate that the mechanical behavior is acceptable, and the level of vibrations induced by the compressed air circulation at different regions of the irradiation device is low and insufficient to generate non-allowable stresses and deformations.

A thermal hydraulic analysis using the CFD method and ANSYS Fluent was done. The results of the calculations show that the maximum temperatures reached by the second silicon ingot irradiated in the heavy water reflector region are of 374.12 and 439.97 K for the coolant flow rates of 30 and 10 m^3/h, respectively. Both maximum temperatures obtained are below the limit value of 453.15 K. The result also shows, from the coolant circulation analysis, that there is no blockage or turbulences which disturb the normal movement of the coolant. The streamlines of the coolant at the orifices and singularities of the irradiation device do not have a great influence on the flow.

Other factors are to be considered to determine the appropriate and final cooling flow rate, mainly the minimal rate at which radioactive argon-41 is produced upon the passage of the compressed air coolant through the Es-Salam reactor core.

Authors prospected to further enhance the design of cooling system in order to decrease the hottest ingot temperature below 373.5 K. At this temperature, we can obtain a doped silicon with high electrical performance, which can be used for large applications.

Acknowledgements Authors are thankful to all the personnel involved in the design, fabrication, and testing/inspection of the irradiation device prototype for the NTD-Si around the Es-Salam research reactor.

References

1. Silicon Transmutation Doping Techniques and Practices. IAEA-TECDOC-456, (1988)
2. X. Li, H. Gerstenberg, I. Neuhaus, Silicon doping system at the research reactor FRM II. Appl. Radiat. Isot. **67**, 1220–1224 (2009). https://doi.org/10.1016/j.apradiso.2009.02.017
3. Neutron Transmutation Doping of Silicon at Research Reactors. IAEA-TECDOC-1681(2012)
4. M.S. Kim, C.S. Lee, S.Y. Oh et al., Radial uniformity of neutron irradiation in silicon ingots for neutron transmutation doping at HANARO. Nucl. Eng. Technol. **38**(1), 93–98 (2006)
5. W. Carbonari, W. Pendl Jr., J.R. Sebastião et al., An irradiation rig for neutron transmutation doping of silicon in the IEA-R1

research reactor. Nucl. Instrum. Methods **83**(1-2), 157–162 (1993). https://doi.org/10.1016/0168-583X(93)95920-Z
6. S. Sheibani, F. Moattar, M. Ghannadi Maragheh et al., Investigation of a simple and efficient method for silicon neutron transmutation doping process in Tehran research reactor. Ann. Nucl. Energy **29**(10), 1195–1208 (2002). https://doi.org/10.1016/S0306-4549(01)00100-1
7. S.S. Abdellatief, M. Osman, S.A. Agamy et al., Design of large sample silicon ingots irradiation facilities using MCNP5. Ann. Nucl. Energy **80**, 40–42 (2015). https://doi.org/10.1016/j.anucene.2015.01.018
8. M. Yagi, M. Watanabe, K. Ohyama et al., Conceptual design of experimental equipment for large-diameter NTD-Si. Appl. Radiat. Isot. **67**(7–8), 1225–1229 (2009). https://doi.org/10.1016/j.apradiso.2009.02.018
9. A.M. Sultan, E. Elsherbiny, M. Sobhy, Method for neutron transmutation doping of silicon in research reactors. Ann. Nucl. Energy **22**(5), 303–310 (1995). https://doi.org/10.1016/0306-4549(94)00063-K
10. Y.Z. Cao, J.J. Guo, The development of NTD technology in the institute of atomic energy, in *Neutron Transmutation Doping of Semiconductor Materials*, ed. by R.D. Larrabee (Plenum Press, New York, 1984), pp. 115–126. https://doi.org/10.1007/978-1-4613-2695-3. ISBN 978-1-4612-9675-1
11. C.A. Landos, Defect states in electron-bombarded n-type silicon. Phys. Status Solidi (a) **113**(2), 503–510 (1989). https://doi.org/10.1002/pssa.2211130231
12. V. Bondarenko, R. Krause-Rehberg, H. Feick et al., Defects in FZ-silicon after neutron irradiation-A positron annihilation and photoluminescence study. J. Mater. Sci. **39**(3), 919–923 (2004). https://doi.org/10.1023/B:JMSC.0000012922.58713.37
13. M. Abbaci, O. Meglali, A. Saim et al., The effect of neutron irradiation defects on electrical resistivity in FZ-silicon samples irradiated at Es-Salam research reactor. Nucl. Instrum. Methods B **251**(1), 167–170 (2006). https://doi.org/10.1016/j.nimb.2006.06.018
14. N. Osmani, L. Guerbous, A. Boucena, Structural, topological, electrical and luminescence properties of CZ-silicon (CZ-Si) irradiated by neutrons. Appl. Phys. A **124**, 709 (2018). https://doi.org/10.1007/s00339-018-2128-x
15. M. Salhi, M. Abbaci, T. Zidi et al., Techniques and Nuclear Applications around Es Salam Reactor, Status and Future Potential. IAEA-TECDOC 1715 (2013)
16. Brüel & Kjaer (ed.), *Analyse structurelle: 2e partie: Analyse modale et simulation, Document pédagogique* (K. Larsen & Son A/S, Naerum, 1989)
17. Brüel & Kjaer (ed.), *Mechanical Vibration and Shock Measurements* (K. Larsen & Son A/S, Naerum, 1984). ISBN 87-87355-34-5
18. Brüel & Kjaer (ed.), *Essais structurels: 1ère partie: Mesures de mobilité, Document pédagogique* (K. Larsen & Son A/S, Naerum, 1988)
19. Process Piping, ASME code for pressure piping, B31 ASME B31.3-2002 [Revision of ASME 831.3-1999], Date of Issuance: April 30, 2002-Table A-1 (2002)
20. R. Dehn, Measurement of Gamma Heating in DFR. Nucl. Instrum. Methods **36**, 141–152 (1965). https://doi.org/10.1016/0029-554x(65)90416-7
21. F.T. Binford, Gamma-ray heating in BSR. Nucleonics **15**(3), 93–97 (1957)
22. R.E. Schreiber, R.J. Allio, Gamma heating in reactor. Nucleonics **22**, 120–125 (1964)
23. K. Heydorn, K. Andresen, Neutron Transmutation Doping of Silicon at RISO National Laboratory, IAEA-TECDOC-456, (1988)
24. J. Koziel, K. Pytel, 1985, Neutron Doped Silicon in Polish Research Reactors, IAEA-TECDOC-456, (1988)
25. M.S. Kim, S.Y. Hwang, H.S. Jung, et al., Measurements of Nuclear Heating Rate and Neutron Flux in HANARO CN Hole for Designing the Moderator Cell of Cold Neutron Source. RRFM-IGOOR (2007)
26. Fluent 14.5.0. Fluent user's guide. USA: ANSYS, Inc (2012)
27. M. Salhi, S.E.H. Abaidia, B. Mohammedi, S. Laouar, Cooling enhancement of planar-balanced magnetron cathode. Nucl. Sci. Tech. **28**, 111 (2017). https://doi.org/10.1007/s41365-017-0271-2